

## Article

# Intelligent Contact Force Regulation of Pantograph–Catenary Based on Novel Type-Reduction Technology

Tsung-Chih Lin <sup>1</sup>, Chien-Wen Sun <sup>1</sup>, Yu-Chen Lin <sup>2,\*</sup>  and Majid Moradi Zirkohi <sup>3</sup>

<sup>1</sup> Department of Electronic Engineering, Feng-Chia University, Taichung 40724, Taiwan; tclin@fcu.edu.tw (T.-C.L.); M1003657@o365.fcu.edu.tw (C.-W.S.)

<sup>2</sup> Department of Automatic Control Engineering, Feng-Chia University, Taichung 40724, Taiwan

<sup>3</sup> Department of Electrical Engineering, Behbahan Khatam Alanbia University of Technology, Behbahan 47189-63616, Iran; moradi@bkatu.ac.ir

\* Correspondence: yuchlin@fcu.edu.tw

**Abstract:** In this paper, an intelligent control scheme is proposed to suppress vibrations between the pantograph and the catenary by regulating the contact force to a reference value, thereby achieving stable current collection. In order to reduce the computational cost, an interval Type-2 adaptive fuzzy logic control with the Moradi–Zirkohi–Lin type reduction method is applied to deal with model uncertainties and exterior interference. Based on a simplified pantograph–catenary system model, the comparative simulation results show that variation of the contact force can be attenuated and variation disturbances can be repressed simultaneously. Furthermore, in terms of computational burden, the proposed type reduction method outperforms other type reduction methods.

**Keywords:** contact force; pantograph; catenary; Moradi–Zirkohi–Lin (MZL) algorithm; intelligent control



**Citation:** Lin, T.-C.; Sun, C.-W.; Lin, Y.-C.; Zirkohi, M.M. Intelligent Contact Force Regulation of Pantograph–Catenary Based on Novel Type-Reduction Technology. *Electronics* **2022**, *11*, 132. <https://doi.org/10.3390/electronics11010132>

Academic Editor: Kalyana C. Veluvolu

Received: 3 December 2021

Accepted: 22 December 2021

Published: 1 January 2022

**Publisher's Note:** MDPI stays neutral with regard to jurisdictional claims in published maps and institutional affiliations.



**Copyright:** © 2022 by the authors. Licensee MDPI, Basel, Switzerland. This article is an open access article distributed under the terms and conditions of the Creative Commons Attribution (CC BY) license (<https://creativecommons.org/licenses/by/4.0/>).

## 1. Introduction

Railway electrification systems that transmit electrical energy from the traction substation to the moving high-speed trains are an efficient alternative to highway and air transportation. The vital subsystem of high-speed railways is the pantograph–catenary system (PCS). When the train moves, the pantograph on its roof slides along and sends electrical current from contact wires, the so-called catenary, to the train motors. The catenary lines are fixed to the irregular-interval support point along the railway line. Moreover, an appropriate contact force between the pantograph and the catenary makes the current collection process effective. However, some main factors affect the contact force between the pantograph and the catenary. To keep the contact force stable, the system output feedback considers the stiffness of the contact wires along each span, the speed of the train, and the distance of adjacent catenary lines. Unfortunately, this may result in loss of contact, wear, and arc, which can severely damage the pantograph and the catenary, whether or not the contact force is too large or too small. Generally, the quality of electric transmission is directly dependent on the interaction performance between the pantograph and the catenary.

Some research results focused on pantograph–catenary structure analysis and experimental aspects have been published. The vertical effect of the vehicle–track vibration on the pantograph–catenary interaction was presented in [1], and both pantograph–catenary and the vehicle–track models were conducted in [2]. The contact wire irregularity stochastic and effect on high-speed railway pantograph–catenary interaction was analyzed in [1]. The dynamic characteristics of the pantograph and catenary components, the systems' dynamic properties, and the environmental influences on the pantograph–catenary interaction were demonstrated in the review article [3]. The simulation of pantograph–catenary interaction benchmarks proposed by researchers from nine countries across Europe and

Asia was accomplished in [4]. Meanwhile, [5] describes line testing methods for the certification of pantographs and catenaries and covers the reliability and availability of the pantograph–overhead line system and life-cycle costs. The effect of locomotive vibrations on pantograph–catenary interactions is investigated in [6]. A pantograph test rig developed for fault detection and diagnosis of high-speed pantograph dynamic behavior is provided in [7]. In this paper, we focus attention on the content of pantograph–catenary dynamics and the main objective to provide a novel type reduction (TR) technology for intelligent contact force regulation of the PCS.

Therefore, to effectively decrease the uncertain fluctuation of the contact force, the dynamic uplift force which is applied to pantograph frame by actuator plays an important part in the PCS. In the previous research, three methods achieve uniformity of the contact force. One is to consider the PCS in detail, including uncertain factors. In [8], performance to evaluate the contact quality adopted the dynamic behavior of the pantograph based on a multibody dynamics theory. In [9], contact resistance temperature distribution and microstructure were analyzed to address the evolutionary process of the sliding electric contact of the PCS. Meeting maintenance requirements by using automatic intelligent detection was also analyzed. In [10], online intelligent perception of the adaptive parameter PCS status was proposed using robust positioning of the PCS image contact point. In [11], automatically extracting the contact point combined with the deep pantograph network under complex backgrounds was proposed. Another proposal was the simple and effective concept of active control of PCS. The control strategy robustly overcame external disturbances by using a linear time-varying uncertain system [12]. A combination of a backstepping robust controller [13], a model predictive controller [14], and an optimal controller [15] made the fluctuation of the contact force achieve minimization in the amplitude of the oscillations with good tracking performance. To regulate the fluctuation of the contact force, it is very important to apply adequate uplift force.

By using the advantages of fuzzy logic control (FLC) [16], intelligent management systems have been used for active control of PCS [17–19]. Although Type-1 fuzzy logic controllers (T1FLCs) have been successfully applied in many application, they cannot fully handle linguistic uncertainties and noisy training data [20]. Fortunately, the interval Type-2 fuzzy logic system (IT2FLS), bound from above and below by two Type-1 fuzzy sets (T1FSs), also called the footprint of uncertainty (FOU), is an extension of the concept of T1FSs. Hence, IT2FLSs can deal with uncertain parameters, modeling vagueness, linguistic uncertainties, and unreliability of information. However, Type-2 fuzzy logic system require a large computational cost (CC). Up to now, many iterative approaches for implementing TR for interval Type-2 fuzzy sets (IT2FSs) have been proposed [21,22]. Much research has been dedicated to providing non-iterative methods to make the effective implementation of the IT2FLS easier, such as the uncertainty bound (UB) method [23], the Nagar–Bardini (NB) method [24], and Begian–Melek–Mendel (BMM) algorithms [25]. A novel and non-iterative TR method using the Moradi–Zirkohi–Lin (MZL) algorithms [26] was created to simultaneously reduce the computational burden and ensure accuracy.

In this paper, an intelligent contact force regulator incorporating MZL algorithms is presented to deal with oscillations produced from uncertain stiffness and to govern the contact force to a pre-specified reference value. Meanwhile, comparative simulations were used to confirm that the proposed TR method outperforms other TR methods.

The rest of this paper is organized as follows: Section 2 describes the simplified PCS model and problem formulation. Section 3 develops the intelligent contact force regulation with the MZL TR method. Section 4 provides the comparative simulation results. Section 5 gives the conclusion is given.

## 2. A Brief Description of the PCS Mathematical Model and Problem Formulation

The dynamics of a PCS are expressed in two common type models: multi-body and lumped-mass. The former is complex and high-computation-time; the latter is relatively simple, standard, and composed of a kinematical chain with elastic joints. Moreover, the

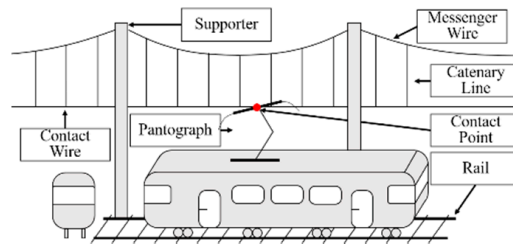
lumped-parameters model is discussed in much research to test the performance of the controller [13,18,19,27]. Therefore, this paper focuses on the linear lumped-mass model with two degrees of freedom; the motion equation of the PCS model is shown in Figure 1 [18,19].

$$m_f \ddot{x}_f(t) + c_f(\dot{x}_f(t)) + c_h(\dot{x}_f(t) - \dot{x}_h(t)) + k_h(x_f(t) - x_h(t)) = F_{up} \tag{1}$$

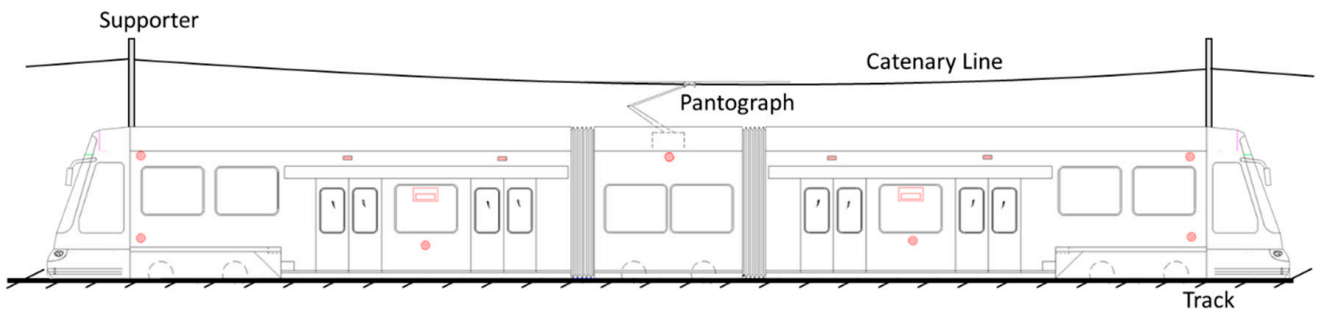
$$m_h \ddot{x}_h(t) + c_h(\dot{x}_h(t) - \dot{x}_f(t)) + k_h(x_h(t) - x_f(t)) + k_{pan}(x_h(t) - x_{cat}(t)) = 0 \tag{2}$$

$$k_{pan}(x_{cat}(t) - x_h(t)) + k_{cat}x_{cat}(t) = 0 \tag{3}$$

where  $F_{up}(t)$  and  $F_c(t)$  are the dynamic uplift force (input) and the contact force (output) of the PCS, respectively. The PCS parameters are listed in Table 1.



(a)



(b)

**Figure 1.** The prototype of a light rail vehicle. (a) Pantograph–catenary system components; (b) lumped-mass model. Reprinted with permission from ref. [18]. Copyright 2016 IEEE.

**Table 1.** Pantograph–catenary system parameter values.

Parameters	Displacement	Speed	Mass	Viscous Damping Coefficient	Stiffness of Suspension
Pantograph head	$x_h$	$\dot{x}_h$	$m_h$	$c_h$	$k_h$
Pantograph frame	$x_f$	$\dot{x}_f$	$m_f$	$c_f$	
Pantograph shoe					$k_{pan}$
Catenary	$x_{cat}$				$k_{cat}$

If state variables are defined as  $x_1 = x_h$ ,  $x_2 = \dot{x}_1$ ,  $x_3 = x_f$ , and  $x_4 = \dot{x}_3$ , the state-space representation of the PCS model can be given as

$$\dot{x}(t) = \begin{bmatrix} 0 & 1 & 0 & 0 \\ \frac{1}{m_h} \left( \frac{-k_{pan}k_{cat}}{k_{pan}+k_{cat}} - k_h \right) & -\frac{c_h}{m_h} & \frac{k_h}{m_h} & \frac{c_h}{m_h} \\ 0 & 0 & 0 & 1 \\ \frac{k_h}{m_f} & \frac{c_h}{m_f} & -\frac{k_h}{m_f} & -\frac{c_f+c_h}{m_f} \end{bmatrix} x(t) + \begin{bmatrix} 0 \\ 0 \\ 0 \\ \frac{1}{m_f} \end{bmatrix} F_{up}(t) \tag{4}$$

$$F_c(t) = \left[ \frac{k_{pan}k_{cat}}{k_{pan} + k_{cat}} \quad 0 \quad 0 \quad 0 \right] x(t) = \frac{k_{pan}k_{cat}}{k_{pan} + k_{cat}} x_1(t) \tag{5}$$

where  $x(t) = [x_1(t), x_2(t), x_3(t), x_4(t)]^T$ . The main objective is to design the dynamic uplift force  $F_{up}(t)$  to regulate the contact force  $F_c(t)$  to the prescribed constant value  $F_{cd}(t) = 100$  N. If the time-varying stiffness of the catenary influenced by the stiffness-variation coefficient  $\alpha$ , the operational speed of train  $V$ , and the length in a span  $L$  are considered, the contact force (5) will be rewritten as

$$F_c(t) = \frac{k_{pan}k_{cat}}{k_{pan} + k_{cat}} \left( 1 + \alpha \cos\left(\frac{2\pi V}{L} t\right) \right) x_1(t) \tag{6}$$

In this paper, using the novel MZL TR algorithm [26] to lower CC and to fully handle or accommodate linguistic and numerical uncertainties, the interval Type-2 adaptive fuzzy logic control (IT2AFLC) incorporating with the identifier is developed to suppress the vibration resulting from the stiffness-variation coefficient  $\alpha$ , the operational speed of train  $V$ , and the length in a span  $L$ .

Remark: It is well known that stiffness variation and wave propagation in catenaries are the main sources of contact loss between the pantograph and catenary [28]. Particularly, wave reflection becomes a major cause for the loss of contact when the speed of the rail vehicle is above 250 km/h. However, the maximum speed of the rail vehicle in our model is 70 km/h and the wave propagation effect can be neglected.

### 3. Intelligent Controller Design

The objective of the controller is to design an adequate uplift force to effectively regulate the uncertain fluctuation of the contact force  $F_c(t)$  to the desired constant value  $F_{cd}(t) = 100$  N, thereby achieving stable current collection. Based on the IT2AFLC incorporating the interval Type-2 adaptive fuzzy neural network identifier (IT2AFNNI) to predict the contact force used to tune the design parameters of the IT2AFLC by a back propagation (BP) algorithm, the intelligent control scheme with output feedback including uncertain stiffness is as shown in Figure 2.

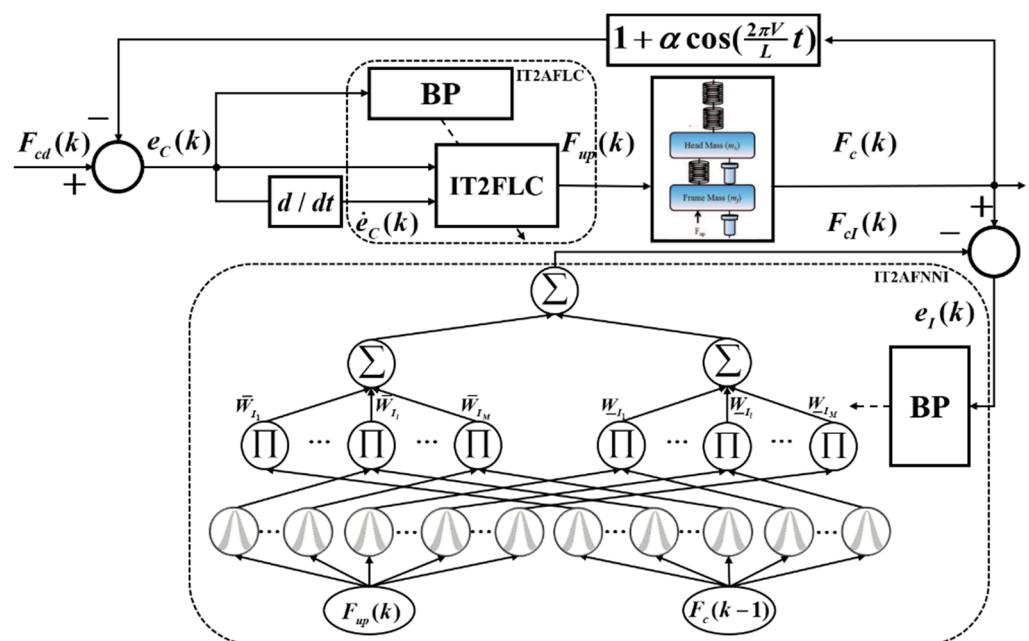


Figure 2. Block diagram of the proposed intelligent IT2AFLC scheme.

To begin with, the proposed control configuration includes two structures, IT2AFNNI and IT2AFLC; the details of the procedures are illustrated as follows.

### 3.1. Training Algorithm for IT2AFNNI

The structure of IT2AFNNI is as shown in Figure 2 and the two inputs are  $F_{up}(k)$  and  $F_c(k-1)$ . The output is the predicted contact force  $F_{cI}(k)$  used to replace  $F_c(k)$  in the regulation phase. In order to train the IT2AFNNI, the performance index (PI) is defined as

$$J_I(k) = \frac{1}{2}(e_I(k))^2 = \frac{1}{2}(F_c(k) - F_{cI}(k))^2 \quad (7)$$

The BP algorithm used to adjust the weights of the IT2AFNNI by minimizing the PI is briefly described as

$$W_I(k+1) = W_I(k) + \Delta W_I(k) = W_I(k) + \eta_I \left( -\frac{\partial J_I(k)}{\partial W_I} \right) \quad (8)$$

By using the chain rule, (8) can be rewritten as

$$W_I(k+1) = W_I(k) + \eta_I \left( -\frac{\partial J_I(k)}{\partial e_I(k)} \frac{\partial e_I(k)}{\partial F_{cI}(k)} \frac{\partial F_{cI}(k)}{\partial W_I} \right) \quad (9)$$

where  $e_I(k) = F_c(k) - F_{cI}(k)$  is the training error,  $\eta_I$  is the learning rate, and  $W_I$  is the output weight. Subscript  $I$  symbolizes the identifier.

### 3.2. Training Algorithm for IT2AFLC

$e_C(k)$  and  $\dot{e}_C(k)$  are two inputs of the IT2AFLC, as shown in Figure 2. The output is contact force  $F_c(k)$ . The PI used to train the IT2AFLC to regulate the contact force is defined as

$$J_C(k) = \frac{1}{2}(e_C(k))^2 = \frac{1}{2}(F_{cd}(k) - F_c(k))^2 \quad (10)$$

To update the weights of the IT2AFLC by attenuating the PI, the BP algorithm is briefly described as

$$W_C(k+1) = W_C(k) + \Delta W_C(k) = W_C(k) + \eta_C \left( -\frac{\partial J_C(k)}{\partial W_C} \right) \quad (11)$$

Based on the chain rule, (11) can be rewritten as

$$W_C(k+1) = W_C(k) + \eta_C \left( -\frac{\partial J_C(k)}{\partial e_C(k)} \frac{\partial e_C(k)}{\partial F_c(k)} \frac{\partial F_c(k)}{\partial F_{up}(k)} \frac{\partial F_{up}(k)}{\partial W_C} \right) \quad (12)$$

where  $e_C(k) = F_{cd}(k) - F_c(k)$  is the regulation error,  $\eta_C$  is the learning rate, and  $W_C$  is the output weight. Subscript  $C$  denotes the controller. The system sensitivity  $\frac{\partial F_c(k)}{\partial F_{up}(k)}$  must be known in order to update the output weights in (12) to guarantee the convergence of the IT2FLC. The IT2AFNNI can achieve this goal by replacing  $\frac{\partial F_c(k)}{\partial F_{up}(k)}$  with  $\frac{\partial F_{cI}(k)}{\partial F_{up}(k)}$  and (12) can be rewritten as

$$W_C(k+1) = W_C(k) + \eta_C \left( -\frac{\partial J_C(k)}{\partial e_C(k)} \frac{\partial e_C(k)}{\partial F_c(k)} \frac{\partial F_{cI}(k)}{\partial F_{up}(k)} \frac{\partial F_{up}(k)}{\partial W_C} \right) \quad (13)$$

### 3.3. Main Results

The IT2AFLC with the MZL TR method is presented to suppress the vibration between the pantograph and the catenary and to deal with the uncertainties resulted from the noisy training data, noisy measurements, and linguistic uncertainties. It is a non-iterative algorithm which can reduce CC and ensure accuracy without computing the center of IT2FLS by sorting weights.

To start with, consider a Type-2 FLS having  $n$  inputs  $x_1 \in X_1, \dots, x_n \in X_n$  and one output  $y \in Y$ . The Type-2 fuzzy rule base consists of a collection of IF-THEN rules. The

rule of a Type-2 relation between the input space  $X_1 \times X_2 \times \dots \times X_n$  and the output space  $Y$  can be expressed as

$$R^l : \text{IF } x_1 \text{ is } \tilde{F}_1^l \text{ and } \dots \text{ and } x_n \text{ is } \tilde{F}_n^l, \text{ THEN } y \text{ is } \tilde{W}^l, l = 1, 2, \dots, M \quad (14)$$

where  $\tilde{F}_j^l$  are antecedent Type-2 sets ( $j = 1, 2, \dots, n$ ) and  $\tilde{W}^l$  are consequent Type-2 sets. Let  $f^i \in \tilde{F}^i \equiv [\underline{f}^i, \bar{f}^i]$ ,  $\underline{f}^i$  and  $\bar{f}^i$  are the lower and upper bounds of the firing strength of the  $i$ th rule of the IT2FLSs, and  $y^i \in Y^i \equiv [\underline{y}^i, \bar{y}^i]$ ,  $\underline{y}^i$  and  $\bar{y}^i$  are the lower and upper bounds of the interval sets considered for the consequent part of the  $i$ th rule of the IT2FLSs.

The MZL TR algorithm is described in Table 2.

**Table 2.** The Moradi–Zirhoji–Lin type reduction algorithm.

Computing $y_l$	Computing $y_r$
$W_{avg} = \frac{\sum_{i=1}^M \bar{f}^i + \sum_{i=1}^M \underline{f}^i}{2}$	
$p_l^i = \begin{cases} \underline{y}^i & \text{if } \underline{y}^i > 0 \\ 0 & \text{if } \underline{y}^i \leq 0 \end{cases}, q_l^i = \begin{cases} \underline{y}^i & \text{if } \underline{y}^i < 0 \\ 0 & \text{if } \underline{y}^i \geq 0 \end{cases}$	$\bar{p}_r^i = \begin{cases} \bar{y}^i & \text{if } \bar{y}^i > 0 \\ 0 & \text{if } \bar{y}^i \leq 0 \end{cases}, \bar{q}_r^i = \begin{cases} \bar{y}^i & \text{if } \bar{y}^i < 0 \\ 0 & \text{if } \bar{y}^i \geq 0 \end{cases}$
Match the firing strength $f^i$ with their respective weights $\underline{y}^i$	Match the firing strength $f^i$ with their respective weights $\bar{y}^i$
$b_l^i = \begin{cases} \underline{f}^i & \text{if } \underline{y}^i > 0 \\ 0 & \text{if } \underline{y}^i \leq 0 \end{cases}, \bar{b}_l^i = \begin{cases} \bar{f}^i & \text{if } \underline{y}^i > 0 \\ 0 & \text{if } \underline{y}^i \leq 0 \end{cases}$	$\bar{b}_r^i = \begin{cases} \underline{f}^i & \text{if } \bar{y}^i > 0 \\ 0 & \text{if } \bar{y}^i \leq 0 \end{cases}, \bar{b}_r^i = \begin{cases} \bar{f}^i & \text{if } \bar{y}^i > 0 \\ 0 & \text{if } \bar{y}^i \leq 0 \end{cases}$
$h_l^i = \begin{cases} \underline{f}^i & \text{if } \underline{y}^i < 0 \\ 0 & \text{if } \underline{y}^i \geq 0 \end{cases}, \bar{h}_l^i = \begin{cases} \bar{f}^i & \text{if } \underline{y}^i < 0 \\ 0 & \text{if } \underline{y}^i \geq 0 \end{cases}$	$\bar{h}_r^i = \begin{cases} \underline{f}^i & \text{if } \bar{y}^i < 0 \\ 0 & \text{if } \bar{y}^i \geq 0 \end{cases}, \bar{h}_r^i = \begin{cases} \bar{f}^i & \text{if } \bar{y}^i < 0 \\ 0 & \text{if } \bar{y}^i \geq 0 \end{cases}$
$[A_l^1 \ A_l^2] = [\sum_{i=1}^M p_l^i b_l^i \ \sum_{i=1}^M p_l^i \bar{b}_l^i]$	$[A_r^1 \ A_r^2] = [\sum_{i=1}^M \bar{p}_r^i b_r^i \ \sum_{i=1}^M \bar{p}_r^i \bar{b}_r^i]$
$[B_l^1 \ B_l^2] = [\sum_{i=1}^M q_l^i h_l^i \ \sum_{i=1}^M q_l^i \bar{h}_l^i]$	$[B_r^1 \ B_r^2] = [\sum_{i=1}^M \bar{q}_r^i h_r^i \ \sum_{i=1}^M \bar{q}_r^i \bar{h}_r^i]$
$A_l = [A_l^1 + B_l^1 \ A_l^1 + B_l^2 \ A_l^2 + B_l^1 \ A_l^2 + B_l^2]$	$A_r = [A_r^1 + B_r^1 \ A_r^1 + B_r^2 \ A_r^2 + B_r^1 \ A_r^2 + B_r^2]$
$y'_{l1} = \frac{\min(A_l)}{W_{avg}}, y'_{l2} = \frac{\max(A_l)}{W_{avg}}$	$y'_{r1} = \frac{\min(A_r)}{W_{avg}}, y'_{r2} = \frac{\max(A_r)}{W_{avg}}$
$y_l = \frac{y'_{l1} + y'_{l2}}{2}$	$y_r = \frac{y'_{r1} + y'_{r2}}{2}$
<b>Output <math>y = \frac{y_l + y_r}{2}</math></b>	

To summarize the above analysis, intelligent contact force regulation of PCS based on the MZL TR algorithm is proposed as follows.

Procedure:

Step (1): Specify the membership functions  $\mu_{F_{up}}$  and  $\mu_{F_c}$ , and adjust the output weights of the IT2AFNNI by BP algorithm (9) to predict the contact force  $F_{Cl}(k)$  of the PCS.

Step (2): Specify the membership functions  $\mu_e$ ,  $\mu_{de}$ , and set up the rule table of the IT2AFLC.

Step (3) Incorporate the IT2AFLC with IT2AFNNI based on the MZL algorithm by replacing  $\frac{\partial F_c(k)}{\partial F_{up}(k)}$  with  $\frac{\partial F_{cl}(k)}{\partial F_{up}(k)}$  and using the BP algorithm (13) to tune the output weights of the IT2AFLC to regulate the contact force to the prescribed level, 100N.

### 4. Simulation Results

In order to verify the regulation performance, the control algorithm proposed in this paper was and compared with T1AFLC and passive control. Furthermore, a comparative study with other TR methods is provided. Simulation results show that the advocated control schemes can not only robustly attenuate the uncertain fluctuation of the contact force, but that the CC can also be efficiently reduced.

The parameters of the PCS used in the following simulation [18] are as specified:  $m_h = 9.1$  kg,  $c_h = 130$  Ns/m,  $k_h = 7 \times 10^3$  N/m,  $m_f = 17.2$  kg,  $c_f = 30$  Ns/m,  $k_{cat} = 1.535 \times 10^6$  N/m,  $k_{pan} = 8.23 \times 10^4$  N/m. According to the design procedure, the design is given in the following steps.

Step (1): The membership functions  $\mu_{F_{up}}$  and  $\mu_{F_c}$  for IT2AFNNI are selected as follows and as shown in Figure 3.

$$\mu_{F_{up1}} = \begin{cases} \frac{1}{1+e^{0.5(F_{up}(k)-60)}} & \text{upper bound} \\ \frac{1}{1+e^{0.5(F_{up}(k)-40)}} & \text{lower bound} \end{cases}, \mu_{F_{up2}} = \begin{cases} e^{-\frac{1}{2} \frac{(F_{up}(k)-75)^2}{30^2}} & \text{upper bound} \\ e^{-\frac{1}{2} \frac{(F_{up}(k)-75)^2}{10^2}} & \text{lower bound} \end{cases}$$

$$\mu_{F_{up3}} = \begin{cases} e^{-\frac{1}{2} \frac{(F_{up}(k)-100)^2}{30^2}} & \text{upper bound} \\ e^{-\frac{1}{2} \frac{(F_{up}(k)-100)^2}{10^2}} & \text{lower bound} \end{cases}, \mu_{F_{up4}} = \begin{cases} e^{-\frac{1}{2} \frac{(F_{up}(k)-125)^2}{30^2}} & \text{upper bound} \\ e^{-\frac{1}{2} \frac{(F_{up}(k)-125)^2}{10^2}} & \text{lower bound} \end{cases}$$

$$\mu_{F_{up5}} = \begin{cases} \frac{1}{1+e^{-0.5(F_{up}(k)-140)}} & \text{upper bound} \\ \frac{1}{1+e^{-0.5(F_{up}(k)-160)}} & \text{lower bound} \end{cases}, \mu_{F_{c1}} = \begin{cases} \frac{1}{1+e^{0.5(F_c(k)-60)}} & \text{upper bound} \\ \frac{1}{1+e^{0.5(F_c(k)-40)}} & \text{lower bound} \end{cases}$$

$$\mu_{F_{c2}} = \begin{cases} e^{-\frac{1}{2} \frac{(F_c(k)-75)^2}{40^2}} & \text{upper bound} \\ e^{-\frac{1}{2} \frac{(F_c(k)-75)^2}{20^2}} & \text{lower bound} \end{cases}, \mu_{F_{c3}} = \begin{cases} e^{-\frac{1}{2} \frac{(F_c(k)-100)^2}{40^2}} & \text{upper bound} \\ e^{-\frac{1}{2} \frac{(F_c(k)-100)^2}{20^2}} & \text{lower bound} \end{cases}$$

$$\mu_{F_{c4}} = \begin{cases} e^{-\frac{1}{2} \frac{(F_c(k)-125)^2}{40^2}} & \text{upper bound} \\ e^{-\frac{1}{2} \frac{(F_c(k)-125)^2}{20^2}} & \text{lower bound} \end{cases}, \mu_{F_{c5}} = \begin{cases} \frac{1}{1+e^{-0.5(F_c(k)-140)}} & \text{upper bound} \\ \frac{1}{1+e^{-0.5(F_c(k)-160)}} & \text{lower bound} \end{cases}$$

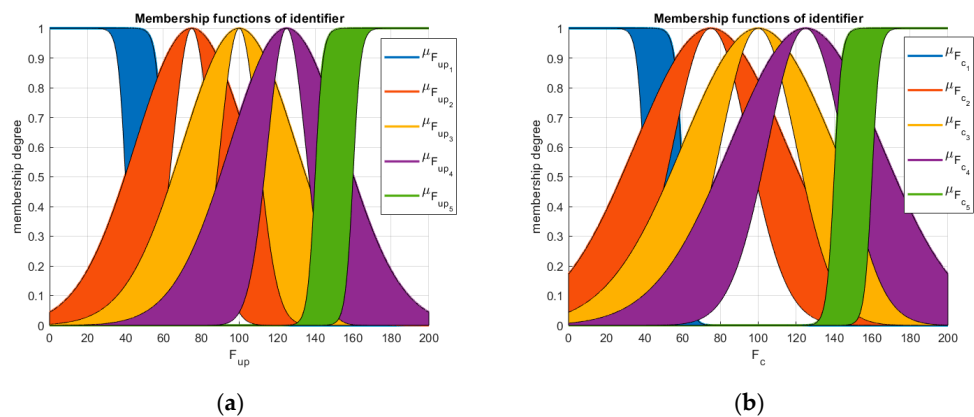


Figure 3. The membership functions for  $\mu_{F_{up}}$  and  $\mu_{F_c}$ . (a) The membership function  $\mu_{F_{up}}$ . (b) The membership function  $\mu_{F_c}$ .

The identification performance is shown in Figure 4 and we can see that the IT2AFNNI can predict the contact force very quickly by (9).

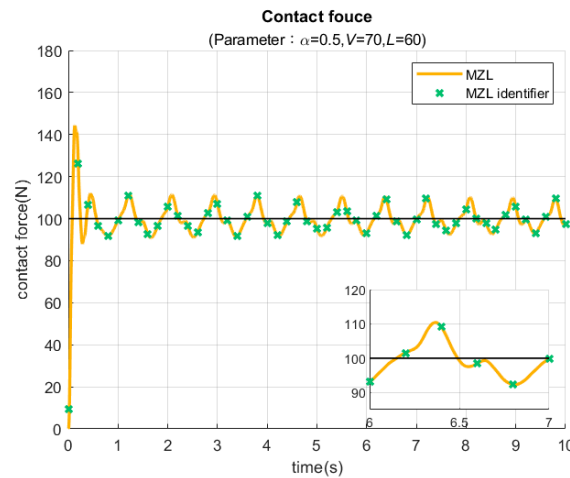


Figure 4. The IT2AFNNI simulation performance.

Step (2) The membership functions  $\mu_e$  and  $\mu_{de}$  for IT2AFLC are selected as shown in Figure 5.

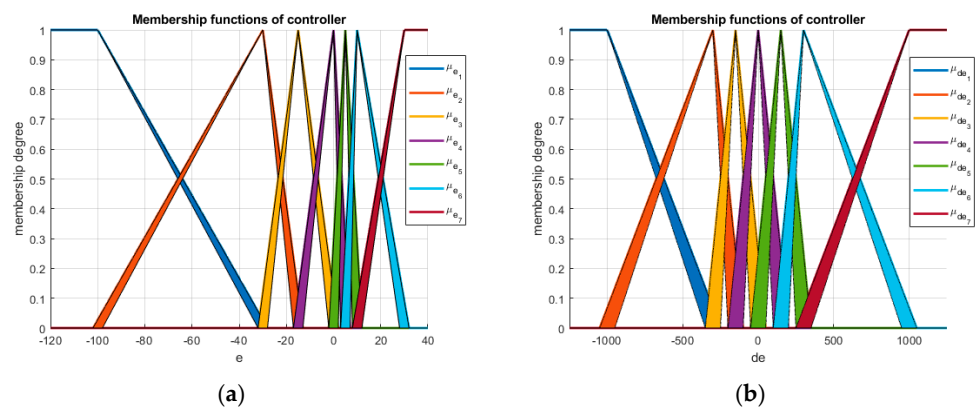


Figure 5. The membership functions for  $\mu_e$  and  $\mu_{de}$ . (a) The membership function  $\mu_e$ . (b) The membership function  $\mu_{de}$ .

Table 3 gives the rule table of the IT2AFLC with  $M = 49$  fuzzy IF-THEN linguistic rules based on the input membership functions  $\mu_e$  and  $\mu_{de}$ , and output membership function  $[y^i, \bar{y}^i] = [w_C^i, \bar{w}_C^i]$ , with the interval weights corresponding rule consequents presented.

Table 3. Interval Type-2 fuzzy rule table.

	$\mu_{de_1}$	$\mu_{de_2}$	$\mu_{de_3}$	$\mu_{de_4}$	$\mu_{de_5}$	$\mu_{de_6}$	$\mu_{de_7}$
$\mu_{e_1}$	(85, 93)	(85, 93)	(90, 95)	(90, 95)	(93, 97)	(95, 99)	(97, 101)
$\mu_{e_2}$	(85, 93)	(90, 95)	(90, 95)	(93, 97)	(95, 99)	(97, 101)	(100, 102)
$\mu_{e_3}$	(90, 95)	(90, 95)	(93, 97)	(95, 99)	(97, 101)	(100, 102)	(101, 103)
$\mu_{e_4}$	(90, 95)	(93, 97)	(95, 99)	(97, 101)	(100, 102)	(101, 103)	(102, 107)
$\mu_{e_5}$	(93, 97)	(95, 99)	(97, 101)	(100, 102)	(101, 103)	(102, 107)	(102, 107)
$\mu_{e_6}$	(95, 99)	(97, 101)	(100, 102)	(101, 103)	(102, 107)	(102, 107)	(105, 125)
$\mu_{e_7}$	(97, 101)	(100, 102)	(101, 103)	(102, 107)	(102, 107)	(105, 125)	(105, 125)

Step (3) In order to obtain the appropriate uplift force  $F_{up}(t)$ , which is the output of the IT2AFLC to force the contact force to the reference  $de_{re}$  level 100 N, the non-iterative MZL

algorithm was used to calculate the center of the IT2FLS to reduce the CC and to ensure accuracy. In accordance with the fuzzy IF-THEN linguistic rule table, the MZL employed to achieve the regulation objective is demonstrated as follows. The most-left uplift force  $F_{up_l}$  and the most-right uplift force  $F_{up_r}$  will be derived from the following process.

- (1) Set average  $W_{avg}$  by

$$W_{avg} = \frac{\sum_{i=1}^{49} \bar{f}^i + \sum_{i=1}^{49} \underline{f}^i}{2} \tag{15}$$

- (2) Determine weights and then match firing strengths of rules

$$\bar{p}_i = \begin{cases} 0 & \bar{w}_C^i \leq 0 \\ \bar{w}_C^i & \bar{w}_C^i > 0 \end{cases}, p_i = \begin{cases} 0 & \underline{w}_C^i \leq 0 \\ \underline{w}_C^i & \underline{w}_C^i > 0 \end{cases}$$

$$\bar{q}_i = \begin{cases} \bar{w}_C^i & \bar{w}_C^i < 0 \\ 0 & \bar{w}_C^i \geq 0 \end{cases}, q_i = \begin{cases} \underline{w}_C^i & \underline{w}_C^i < 0 \\ 0 & \underline{w}_C^i \geq 0 \end{cases}$$

$$\begin{bmatrix} \bar{A}_1 & \bar{A}_2 \\ \underline{A}_1 & \underline{A}_2 \end{bmatrix} = \begin{bmatrix} \sum_{i=1}^{49} \underline{f}^i \bar{p}^i & \sum_{i=1}^{49} \bar{f}^i \bar{p}^i \\ \sum_{i=1}^{49} \underline{f}^i p^i & \sum_{i=1}^{49} \bar{f}^i p^i \end{bmatrix}, \begin{bmatrix} \bar{B}_1 & \bar{B}_2 \\ \underline{B}_1 & \underline{B}_2 \end{bmatrix} = \begin{bmatrix} \sum_{i=1}^{49} \underline{f}^i \bar{q}^i & \sum_{i=1}^{49} \bar{f}^i \bar{q}^i \\ \sum_{i=1}^{49} \underline{f}^i q^i & \sum_{i=1}^{49} \bar{f}^i q^i \end{bmatrix} \tag{16}$$

- (3) Compute all possible combinations

$$A_l = \begin{bmatrix} \bar{A}_1 + \bar{B}_1 & \bar{A}_1 + \bar{B}_2 & \bar{A}_2 + \bar{B}_1 & \bar{A}_2 + \bar{B}_2 \\ \underline{A}_1 + \underline{B}_1 & \underline{A}_1 + \underline{B}_2 & \underline{A}_2 + \underline{B}_1 & \underline{A}_2 + \underline{B}_2 \end{bmatrix}$$

$$A_r = \begin{bmatrix} \bar{A}_1 + \bar{B}_1 & \bar{A}_1 + \bar{B}_2 & \bar{A}_2 + \bar{B}_1 & \bar{A}_2 + \bar{B}_2 \\ \underline{A}_1 + \underline{B}_1 & \underline{A}_1 + \underline{B}_2 & \underline{A}_2 + \underline{B}_1 & \underline{A}_2 + \underline{B}_2 \end{bmatrix} \tag{17}$$

- (4) Compute

$$y'_{l1} = \frac{\min(A_l)}{W_{avg}}, y'_{l2} = \frac{\max(A_l)}{W_{avg}}, y'_{r1} = \frac{\min(A_r)}{W_{avg}}, y'_{r2} = \frac{\max(A_r)}{W_{avg}} \tag{18}$$

- (5) Compute crisp output, uplift force  $F_{up}$

$$y_l = \frac{y'_{l1} + y'_{l2}}{2}, y_r = \frac{y'_{r1} + y'_{r2}}{2} \text{ and } F_{up} = \frac{y_l + y_r}{2} \tag{19}$$

The following two case simulations will be analyzed and discussed:

Case 1:

To check robustness, the comparison between the T1AFLC with interference from a white Gaussian noise with SNR 20 dB, the traditional passive control ( $F_{up}(t) = 100$  N), and the proposed IT2AFLC will be considered. Due to the inclusion of linguistic uncertainty and data noise, the IT2AFLC can more efficiently regulate the contact force than Type-1 adaptive fuzzy logic control (T1AFLC) and the traditional passive control, as shown in Figure 6. The dynamic uplift force is severely unsteady, i.e., much more control effort must be consumed for T1AFLC, resulting in implementation difficulty as shown in Figure 7. In contrast, the control force is stable for IT2AFLC.

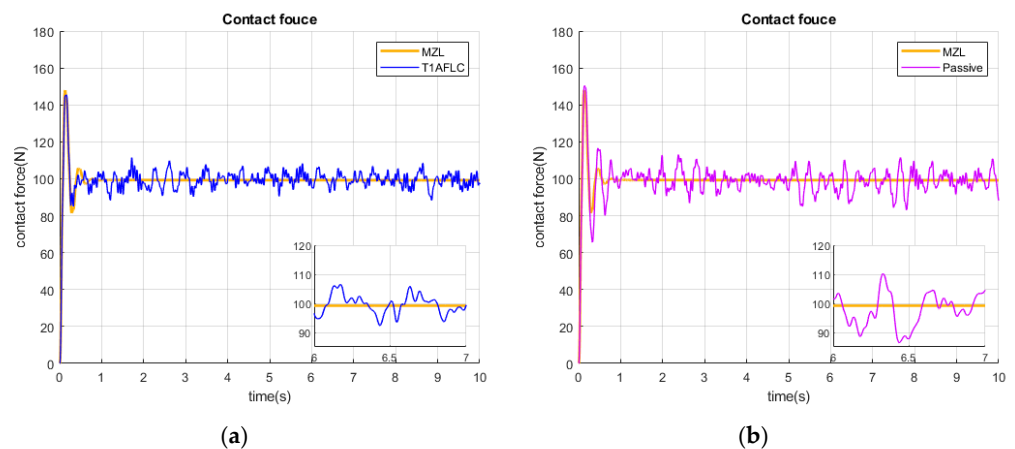


**Figure 6.** The contact force regulation performance. (a) The contact force for T1AFLC and the proposed IT2AFLC. (b) The contact force for passive control and the proposed IT2AFLC.

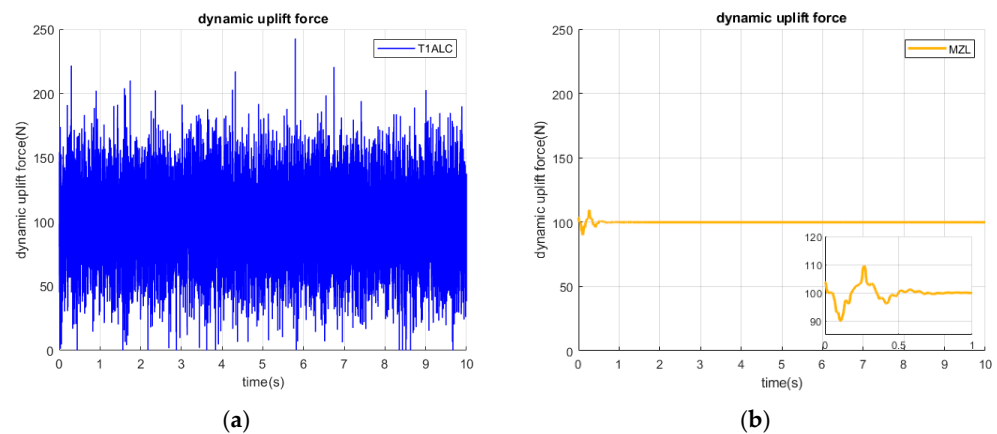


**Figure 7.** The dynamic uplift force. (a) The dynamic uplift force for T1AFLC. (b) The dynamic uplift force for proposed IT2AFLC.

Case 2:

To consider the influence resulting from the time-varying stiffness of the catenary, the feedback signal of contact force  $F_c(t)$  blended with the stiffness-variation coefficient  $\alpha$ , the operational speed of train  $V$ , and the length in a span  $L$  as (6), the vibration suppression efficiency (VSE) [29] will be analyzed and compared between the proposed MZL algorithm, the Karnik–Mendel (KM) algorithm [30–33], and simplified interval Type-2 Takagi–Sugeno–Kang fuzzy systems (IT2 TSK FS) [34–36].

First of all, the VSE is defined as

$$VSE \triangleq \left(1 - \frac{\Phi}{\Phi_0}\right) \cdot 100\% \tag{20}$$

where  $\Phi$  is the amplitude of the steady contact force value and  $\Phi_0 = 2\alpha F_{cd}(t)$  is the amplitude of the contact force by traditional passive control, as shown in Figure 8.

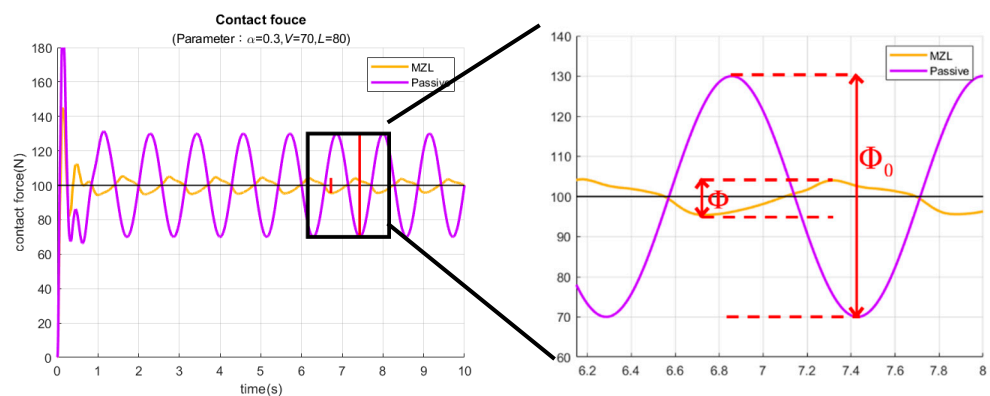


**Figure 8.** The definition of the  $\Phi$  and  $\Phi_0$  for VSE.

Two different sets of the different ( $\alpha = 0.3, V = 70, L = 40$ ) and ( $\alpha = 0.6, V = 70, L = 80$ ) are simulated and analyzed as follows. The contact force regulation performance for IT2AFLC with different three TR methods are almost the same, as shown in Figure 9. Similarly, the vertical position, speed, and acceleration of the pantograph head and frame are definitely the same as those demonstrated in Figures 10 and 11, respectively. Finally, the simplified IT2 algorithm uses larger dynamic uplift force than the proposed MZL algorithm and the KM algorithm, as illustrated in Figure 12.

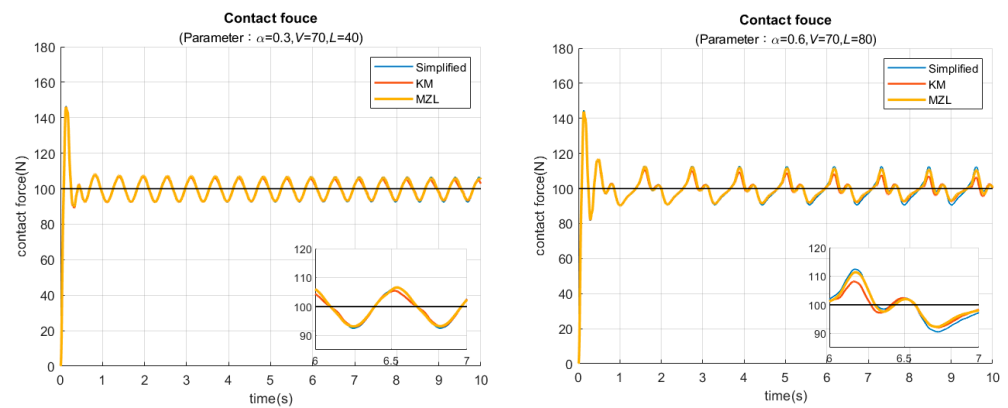


**Figure 9.** The contact force regulation performance for IT2AFLC with three different type reduction methods.

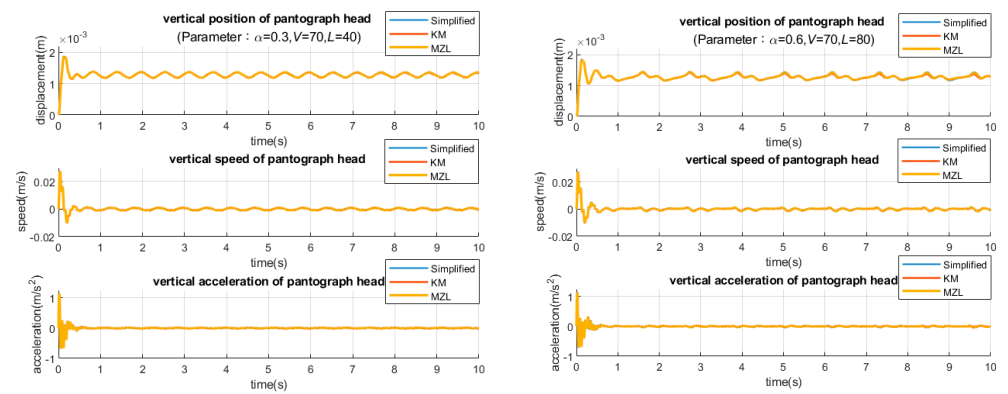


**Figure 10.** The resulting vertical position, velocity, and acceleration of the pantograph head.

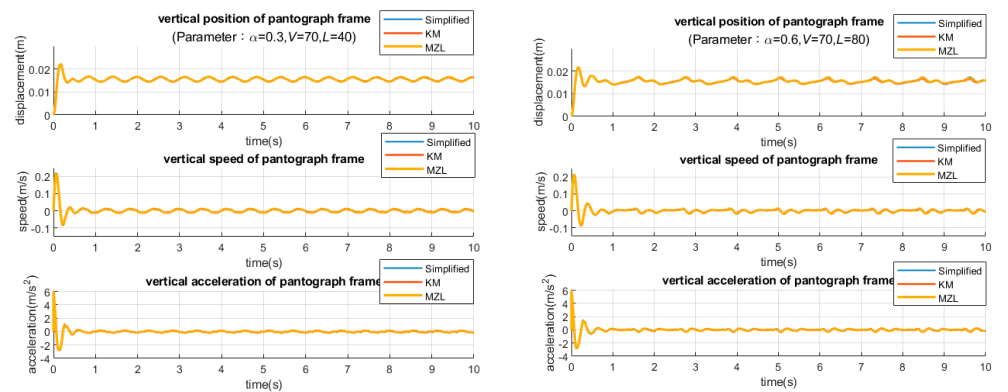


**Figure 11.** The resulting vertical position, velocity, and acceleration of the pantograph frame.

Furthermore, comparative results of the VSE and the CC for  $\alpha = 0.3$ ,  $\alpha = 0.4$ ,  $\alpha = 0.5$ , and  $\alpha = 0.6$ , with speed  $V = 60$  and  $V = 70$  km/hr and  $L$ , are reported in Tables 4 and 5, respectively. To provide a better comparison, the bar-line chart of the data reported in Tables 4 and 5 is also shown in Figure 13. It can be clearly seen that the VSE are very similar for the three different TR algorithms. However, for real-time applications, the computation time is a major factor; therefore, we can notice that the proposed MZL TR algorithm is more operant than the KM algorithm and the simplified IT2 algorithm in terms of contact force regulation accuracy and computational cost.

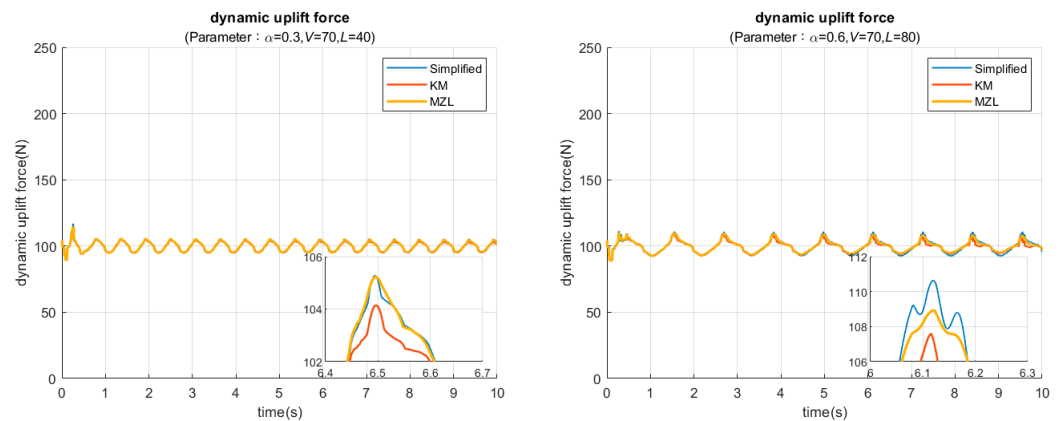


Figure 12. The dynamic uplift force.

Table 4. The comparative results of the vibration suppression efficiency and the computational cost for  $\alpha = 0.3, 0.5$ .

Time-Varying Stiffness	$\alpha$	0.3						0.5					
		V		60		70		60		70			
	L	40	60	80	40	60	80	40	60	80	40	60	80
Simplified	CC (sec)	45.58	45.81	52.01	44.86	45.38	45.25	50.74	43.68	46.43	52.36	44.11	52.29
	VSE (%)	79.22	82.13	84.92	76.30	81.14	83.35	76.68	81.69	86.42	74.06	79.19	84.43
KM	CC (sec)	81.60	80.59	81.05	70.58	80.42	72.11	70.05	77.22	69.91	71.38	70.48	74.40
	VSE (%)	80.44	83.51	85.90	77.36	82.69	84.82	79.48	84.63	88.19	77.16	82.29	87.00
MZL	CC (sec)	<b>24.35</b>	<b>22.54</b>	<b>21.06</b>	<b>25.52</b>	<b>24.43</b>	<b>22.96</b>	<b>23.34</b>	<b>20.84</b>	<b>23.55</b>	<b>27.28</b>	<b>26.31</b>	<b>26.08</b>
	VSE (%)	78.93	82.31	84.85	75.95	81.22	83.59	78.43	82.38	86.21	75.66	80.33	84.51

Table 5. The comparative results of the vibration suppression efficiency and the computational cost for  $\alpha = 0.4, 0.6$ .

Time-Varying Stiffness	$\alpha$	0.4						0.6					
		V		60		70		60		70			
	L	40	60	80	40	60	80	40	60	80	40	60	80
Simplified	CC (sec)	46.72	50.39	51.71	52.36	44.11	52.29	54.49	53.71	45.24	45.67	53.94	54.99
	VSE (%)	78.34	83.40	85.77	75.13	81.84	84.56	75.95	78.36	85.18	73.33	76.16	81.62
KM	CC (sec)	66.30	73.87	66.45	71.38	70.48	74.40	68.82	68.64	77.52	67.03	75.86	77.45
	VSE (%)	80.26	85.65	87.32	77.19	84.04	86.76	79.92	82.14	87.48	78.34	80.44	84.86
MZL	CC (sec)	<b>24.50</b>	<b>19.21</b>	<b>27.16</b>	<b>27.28</b>	<b>26.31</b>	<b>26.08</b>	<b>21.81</b>	<b>23.67</b>	<b>21.20</b>	<b>24.50</b>	<b>23.67</b>	<b>27.16</b>
	VSE (%)	78.84	83.53	85.98	75.62	81.99	84.84	78.34	80.33	85.56	76.91	79.18	82.65

In order to test the effect of parameter variations on the performance of vibration suppression and contact force regulation, the stiffness of the pantograph shoe suspension  $k_{pan}$ , the pan-head suspension  $k_h$ , the catenary suspension  $k_{cat}$ , the viscous damping of the pan-head suspension  $c_h$ , and the frame suspension  $c_f$  were changed from 80% to 120% of their nominal values given in the above simulation. Table 6 summarizes the performance changes when there were  $\pm 20\%$  parameter perturbations in the spring and damping coefficients. The results show excellent contact force regulation and vibration suppression performance robust with our proposed control scheme.

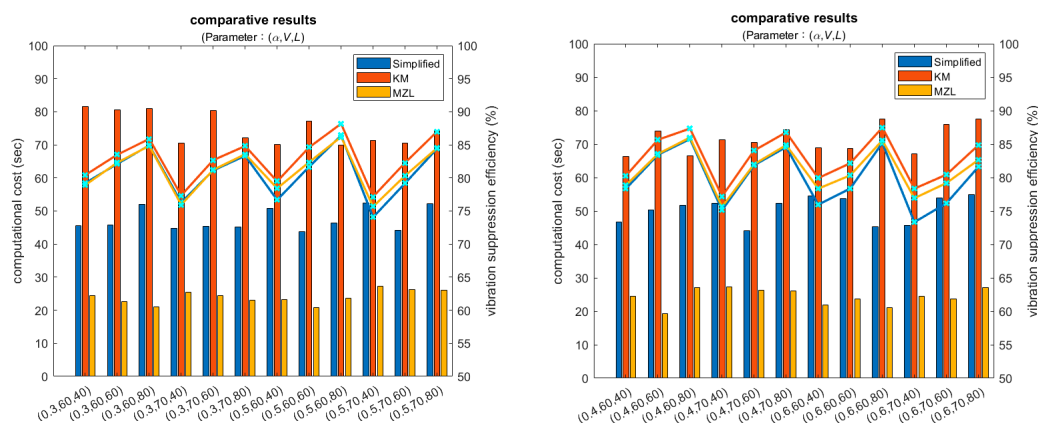


Figure 13. Bar-line chart showing the comparative results (bar—CC, line—VSE).

Table 6. Test of performance robustness.

Item		Contact Force	Variance (%)	VSE(α=0.6, V=70, L=40)	Variance (%)
Nominal		99.9120	0	76.9096	0
Viscous damping coefficient $c_h, c_f$	+20%	99.9202	0.0082	76.6405	0.3499
	−20%	99.9106	0.0014	76.9648	0.0718
Stiffness of suspension $k_h, k_{pan}, k_{cat}$	+20%	99.9105	0.0015	76.0437	1.1259
	−20%	99.9155	0.0035	76.7688	0.1831

### 5. Conclusions

In this paper, based on the MZL TR method, an intelligent control scheme is presented to suppress the vibration between the pantograph and the catenary by regulating the contact force to a reference value. The simple MZL algorithm is used to reduce the computational time cost and to deal with model uncertainties, linguistic uncertainties, and exterior interference; stable current collection can then be achieved. Comparative simulation results show that the vibration of the contact force resulting from the time-varying stiffness of the catenary can be effectively suppressed and the proposed MZL TR algorithm is more efficient than the simplified IT2 structure algorithm, a hybrid structure of four Type-1 fuzzy systems, and the KM TR algorithm, all common iterative algorithms, in regards to accuracy and computational burden. Furthermore, the proposed control scheme will be applied in real life in future experimental implementations.

**Author Contributions:** Conceptualization, T.-C.L.; Data curation, M.M.Z.; Formal analysis, T.-C.L., C.-W.S. and M.M.Z.; Funding acquisition, Y.-C.L.; Investigation, T.-C.L.; Methodology, T.-C.L.; Project administration, Y.-C.L.; Resources, Y.-C.L.; Software, C.-W.S.; Supervision, T.-C.L.; Validation, T.-C.L. and C.-W.S.; Visualization, C.-W.S. and M.M.Z.; Writing—original draft, T.-C.L. and C.-W.S. All authors have read and agreed to the published version of the manuscript.

**Funding:** This research received no external funding.

**Data Availability Statement:** The original contributions presented in the study are included in the article, and further inquiries can be directed to the corresponding author.

**Conflicts of Interest:** The authors declare no conflict of interest.

### References

1. Song, Y.; Liu, Z.; Rønquist, A.; Nāvik, P.; Liu, Z. Contact Wire Irregularity Stochastics and Effect on High-Speed Railway Pantograph–Catenary Interactions. *IEEE Trans. Instrum. Meas.* **2020**, *69*, 8196–8206. [CrossRef]
2. Song, Y.; Wang, Z.; Liu, Z.; Wang, R. A spatial coupling model to study dynamic performance of pantograph-catenary with vehicle-track excitation. *Mech. Syst. Signal Process.* **2021**, *151*, 107336. [CrossRef]

3. Zhang, W.; Zou, D.; Tan, M.; Zhou, N.; Li, R.; Mei, G. Review of pantograph and catenary interaction. *Front. Mech. Eng.* **2018**, *13*, 311–322. [[CrossRef](#)]
4. Bruni, S.; Ambrosio, J.; Carnicero, A.; Cho, Y.H.; Finner, L.; Ikeda, M.; Kwon, S.Y.; Massat, J.-P.; Stichel, S.; Tur, M.; et al. The results of the pantograph–catenary interaction benchmark. *Veh. Syst. Dyn.* **2015**, *53*, 412–435. [[CrossRef](#)]
5. Bruni, S.; Bucca, G.; Carnevale, M.; Collina, A.; Facchinetti, A. Pantograph–catenary interaction: Recent achievements and future research challenges. *Int. J. Rail Transp.* **2018**, *6*, 57–82. [[CrossRef](#)]
6. Zhai, W.M.; Cai, C.B. Effect of Locomotive Vibrations on Pantograph–Catenary System Dynamics. *Veh. Syst. Dyn.* **1998**, *29*, 47–58. [[CrossRef](#)]
7. Xin, T.; Roberts, C.; Weston, P.; Stewart, E. Condition monitoring of railway pantographs to achieve fault detection and fault diagnosis. *Proc. Inst. Mech. Eng. Part F J. Rail Rapid Transit* **2020**, *234*, 289–300. [[CrossRef](#)]
8. Wang, J.; Mei, G. Effect of Pantograph’s Main Structure on the Contact Quality in High-Speed Railway. *Shock. Vib.* **2021**, *2021*, 4037999. [[CrossRef](#)]
9. Wu, G.; Wu, J.; Wei, W.; Zhou, Y.; Yang, Z.; Gao, G. Characteristics of the Sliding Electric Contact of Pantograph/Contact Wire Systems in Electric Railways. *Energies* **2018**, *11*, 17. [[CrossRef](#)]
10. Shen, Y.; Pan, X.; Chang, L. Online Intelligent Perception of Pantograph and Catenary System Status Based on Parameter Adaptation. *Appl. Sci.* **2021**, *11*, 1948. [[CrossRef](#)]
11. Zhang, D.; Gao, S.; Yu, L.; Kang, G.; Zhan, D.; Wei, X. A Robust Pantograph–Catenary Interaction Condition Monitoring Method Based on Deep Convolutional Network. *IEEE Trans. Instrum. Meas.* **2020**, *69*, 1920–1929. [[CrossRef](#)]
12. Wu, T.X.; Brennan, M.J. Active vibration control of a railway pantograph. *Proc. Inst. Mech. Eng. Part F J. Rail Rapid Transit* **1997**, *211*, 117–130. [[CrossRef](#)]
13. Liu, Z.; Liu, Y.; Zhou, N.; Zou, D.; Tu, H. Backstepping Controller Design for Pantograph–Catenary System. *IOP Conf. Ser. Mater. Sci. Eng.* **2018**, *428*, 012045. [[CrossRef](#)]
14. Ioan Chiriac, A.; Constantin Olteanu, S.; Popescu, D. Model Predictive Control Approach for a Pantograph–Catenary System (PAC) Described by a Transfer Function Model. In Proceedings of the 2020 24th International Conference on System Theory, Control and Computing (ICSTCC), Sinaia, Romania, 8–10 October 2020; pp. 733–738.
15. Shudong, W.; Jingbo, G.; Guosheng, G. Research of the active control for high-speed train pantograph. In Proceedings of the 2008 IEEE Conference on Cybernetics and Intelligent Systems, Chengdu, China, 21–24 September 2008; pp. 749–753.
16. Lin, T.-C.; Li, C.-Y.; Chen, P.-F.; Chen, W.-K.; Dey, R.; Balas, M.M.; Olariu, T.; Wong, W.-S. Identifier based intelligent blood glucose concentration regulation for type 1 diabetic patients: An adaptive fuzzy approach. *J. Intell. Fuzzy Syst.* **2020**, *38*, 6175–6184. [[CrossRef](#)]
17. Farhan, M.F.; Shukor, N.S.A.; Ahmad, M.A.; Suid, M.H.; Ghazali, M.R.; Jusof, M.F.M. A simplify fuzzy logic controller design based safe experimentation dynamics for pantograph–catenary system. *Indones. J. Electr. Eng. Comput. Sci.* **2019**, *14*, 903–911. [[CrossRef](#)]
18. Lin, T.-C.; Yeh, J.-L.; Kuo, C.-H.; Lin, Y.-C.; Balas, V.E. Adaptive fuzzy sliding mode active vibration control for rail vehicle pantograph. In Proceedings of the 2016 IEEE International Conference on Fuzzy Systems (FUZZ-IEEE), Vancouver, BC, Canada, 24–29 July 2016; pp. 373–379.
19. Karaköse, E.; Gençoğlu, M.T. Adaptive fuzzy control approach for dynamic pantograph–catenary interaction. In Proceedings of the 15th International Conference MECHATRONIKA, Prague, Czech Republic, 5–7 December 2012; pp. 1–5.
20. Lin, T.-C.; Chen, C.-L. Uncertain nonlinear time delay systems fast and large disturbance rejection based on adaptive interval type-2 fuzzy PI control. In Proceedings of the 2014 IEEE International Conference on Fuzzy Systems (FUZZ-IEEE), Beijing, China, 6–11 July 2014; pp. 647–653.
21. Torshizi, A.D.; Zarandi, M.H.F.; Zakeri, H. On type-reduction of type-2 fuzzy sets: A review. *Appl. Soft Comput.* **2015**, *27*, 614–627. [[CrossRef](#)]
22. Wu, D. Two Differences between Interval Type-2 and Type-1 Fuzzy Logic Controllers: Adaptiveness and Novelty. In *Advances in Type-2 Fuzzy Sets and Systems: Theory and Applications*; Sadeghian, A., Mendel, J.M., Tahayori, H., Eds.; Studies in Fuzziness and Soft Computing; Springer: New York, NY, USA, 2013; pp. 33–48. ISBN 978-1-4614-6666-6.
23. Wu, H.; Mendel, J.M. Uncertainty bounds and their use in the design of interval type-2 fuzzy logic systems. *IEEE Trans. Fuzzy Syst.* **2002**, *10*, 622–639. [[CrossRef](#)]
24. Mendel, J.M.; Liu, X. Simplified Interval Type-2 Fuzzy Logic Systems. *IEEE Trans. Fuzzy Syst.* **2013**, *21*, 1056–1069. [[CrossRef](#)]
25. Begian, M.B.; Melek, W.W.; Mendel, J.M. Stability analysis of type-2 fuzzy systems. In Proceedings of the 2008 IEEE International Conference on Fuzzy Systems (IEEE World Congress on Computational Intelligence), Hong Kong, China, 1–6 June 2008; pp. 947–953.
26. Moradi Zirkohi, M.; Lin, T.-C. An efficient non-iterative method for computing the centroid of an interval type-2 fuzzy set. *J. Intell. Fuzzy Syst.* **2021**, *41*, 2879–2889. [[CrossRef](#)]
27. Rachid, A. Pantograph catenary control and observation using the LMI approach. In Proceedings of the 2011 50th IEEE Conference on Decision and Control and European Control Conference, Orlando, FL, USA, 12–15 December 2011; pp. 2287–2292.
28. Lin, Y.-C.; Shieh, N.-C.; Liu, V.-T. Optimal control for rail vehicle pantograph systems with actuator delays. *IET Control Theory Appl.* **2015**, *9*, 1917–1926. [[CrossRef](#)]

29. Kuo, C.-H. Fuzzy Sliding Mode Active Vibration Control for Tram-Train Pantograph. Master's Thesis, Feng Chia University, Taiwan, China, 2016.
30. Lin, T.-C.; Lin, Y.-C.; Du, Z.; Chen, C.-L. Adaptive Interval Type-2 Fuzzy PI Control for Uncertain Nonlinear Time Delay Systems Fast and Large Disturbance Rejection. *Int. J. Comput. Intell. Control* **2021**, *13*, 24.
31. Lin, T.-C.; Kuo, C.-H.; Balas, V.E. Real-time recurrent interval type-2 fuzzy-neural system identification using uncertainty bounds. In Proceedings of the 2012 IEEE International Conference on Fuzzy Systems, Brisbane, Australia, 10–15 June 2012; pp. 1–8.
32. Wu, D.; Nie, M. Comparison and practical implementation of type-reduction algorithms for type-2 fuzzy sets and systems. In Proceedings of the 2011 IEEE International Conference on Fuzzy Systems (FUZZ-IEEE 2011), Taiwan, China, 27–30 June 2011; pp. 2131–2138.
33. Phan, D.; Bab-Hadiashar, A.; Fayyazi, M.; Hoseinnezhad, R.; Jazar, R.N.; Khayyam, H. Interval Type 2 Fuzzy Logic Control for Energy Management of Hybrid Electric Autonomous Vehicles. *IEEE Trans. Intell. Veh.* **2021**, *6*, 210–220. [[CrossRef](#)]
34. Hassanzadeh, H.R.; Akbarzadeh-T, M.-R.; Akbarzadeh, A.; Rezaei, A. An interval-valued fuzzy controller for complex dynamical systems with application to a 3-PSP parallel robot. *Fuzzy Sets Syst.* **2014**, *235*, 83–100. [[CrossRef](#)]
35. Gordan, H.; Zare, A.; Balochian, S. A Simplified Architecture of Type-2 TSK Fuzzy Logic Controller for Fuzzy Model of Double Inverted Pendulums. *Theory Appl. Math. Comput. Sci.* **2012**, *2*, 20–30.
36. Lin, T.-C.; Balas, V.E.; Lee, T.-Y. Synchronization of uncertain fractional order chaotic systems via adaptive interval type-2 fuzzy sliding mode control. In Proceedings of the 2011 IEEE International Conference on Fuzzy Systems (FUZZ-IEEE 2011), Taiwan, China, 27–30 June 2011; pp. 2882–2889.